ROTOR CASCADE ASSESSMENT AT OFF-DESIGN CONDITION: AN AERODYNAMIC INVESTIGATION ON PLATFORM COOLING

H. Abdeh - G. Barigozzi – N. Franchina

Department of Engineering and Applied Sciences, University of Bergamo, Dalmine, Italy
hamed.abdeh@unibg.it, giovanna.barigozzi@unibg.it, nicoletta.franchina@unibg.it

ABSTRACT

Off-design condition of a rotor blade cascade with and without platform cooling has been experimentally investigated. The ability of the gas turbine to operate down to 50% to 20% of its nominal intake air flow rate has an important consequence in the change in the inlet incidence angle, which was varied from nominal to -20°. Platform cooling through an upstream slot simulating the stator to rotor interface gap was considered. The impact of rotation on purge flow injection was simulated installing fins inside of the slot, to give the coolant flow a tangential direction. Aerodynamic measurements to quantify the cascade aerodynamic loss and secondary flow structures were performed at Ma_{2is} = 0.55, varying the coolant to main flow mass flow ratios (*MFR* %) and the incidence angle. The results show that losses strongly increase with *MFR*. A negative incidence allows a reduction of the overall loss even when coolant is injected with a high *MFR*. The greater the loss reduction the more negative the incidence.

KEYWORDS: Gas Turbine, Platform, Secondary Flows, Incidence Angle

NOMENCLATURE

a	*speed of sound*
C	*blade chord*
H	*blade height*
$H_{12} = \delta/\theta$	*shape factor*
i	*flow incidence angle*
$Ma = U/a$	*Mach number*
$MFR = m_c/m_\infty$	*mass flow rate (%)*
p	*pressure*
$Re_{2,is} = U_{2is}C/\nu$	*isentropic outlet Reynolds number*
s	*blade pitch*
$Tu = u'/U$	*turbulence Intensity (%)*
u, v, w	*velocity Components*
U	*mean velocity*
X, Y, Z	*cascade coordinate system*
w	*slot width*
β	*flow angle*
δ	*boundary layer thickness*
δ^*	*displacement thickness*
γ	*fins inclination angle*
ν	*kinematic viscosity*
Λ_x	*turbulent length scale*
$\zeta = \frac{U_{2is}^2 - U_2^2}{\bar{U}_{2is,ms}^2}$	*kinetic energy loss coefficient*
$\Omega = \Omega_s C/U_1$	*non dimensional stream wise vorticity*

Superscript

$'$	*RMS*
-	*pitch averaged*
=	*mass averaged*

Subscript

ax	*axial*
c	*coolant*
is	*isentropic condition*
ms	*at midspan*
1	*rotor inlet*
2	*rotor exit*
∞	*mainstream*

INTRODUCTION

Recent trends in power generation aim to reduce the environmental impact of anthropic activities since concerns about the irreversible consequences of global warming have grown over the past few years. At the heart of the energy transition scenario is the need to reduce energy-related CO_2 emissions to limit climate change (Ray and De, (2020)). The competitiveness of renewable energies vs. fossil fuels has been increasing, specially concerning electricity generation. Renewable primary energy (excluding hydro) increased by around 5.1 EJ in 2021 over the world, corresponding to an annual growth rate of 15%, stronger than the previous year's 9% (BP Statistical Review of World Energy 2022). The share of renewable energies is expected to further increase in upcoming decade. In the short terms the gas turbine engines will be the partner of renewables playing a vital role in the pathway toward transformation of the global energy sector from fossil-based to zero-carbon energy sources. Gas turbines can be used to absorb energy fluctuations of renewables in the grid, as well as provide immediate emission reductions using carbon-neutral fuels like ammonia, hydrogen, or bio-jet fuel.

To stay competitive in the market, the new generation turbines shall be designed to quickly ramp up and down, start-up and shutdown promptly, and tolerate turndown to low output while complying with emissions regulations. Fast start-up and shutdown, with frequent load adjustments down to reduced minimum load, lead engines to operate under more critical thermo-mechanical conditions with metal distortions that may heavily impact the fluid dynamics of the secondary air system (SAS) and, consequently, of the whole engine.

Better understanding of aero-thermo-mechanical interactions and more accurate predictions of aerodynamics, heat transfer and cooling flows in variable load operating conditions are decisive to modern engine designs. Although transient regimes might represent a significant portion of the working time of industrial gas turbines in the next coming energy production scenario, the knowledge of the behavior in reduced minimum load conditions of typical SAS components, and their interactions with main flow path in view of the deformations of stator/rotor parts, is nowadays limited. Purge air, bled from the latter stages of the compressor, is introduced into the turbine wheel space at low radius before exiting through the rim-seal at the periphery of the discs, immediately upstream of the blade endwall. Labyrinth seals are used as contactless solution to limit as much as possible the leakage between the stationary and rotating components and to control the cooling air supply to the elements laying in the hot gas path. Many studies document the performance of labyrinth seals, mostly reporting discharge coefficient as a function of the pressure ratio data (Bozzi et al. (2011), Szyma´nski et al. (2020)) from which simple 1D design correlations can be argued. The flow through labyrinth seals has been shown to be highly sensitive to geometric variations due to changes in rotational speed and the discharge coefficient varies significantly when the seal clearance is changed by only 2% (Nayak (2020), Fraczek et al. (2016)). Off design flow conditions due to large variations of the clearance must be considered for a further improvement of the SAS system and, consequently, of the whole engine performance.

The sealing flow emerging from the stator to rotor interface gap interacts with the main flow, influencing both aerodynamic and thermal performance of the rotor cascade. An exhaustive review of the available literature on this topic can be found in Barigozzi et al. (2022). Loss for the blade row increases with the purge flow rate (see for example Regina et al. (2015)) due to the strengthening of the horseshoe vortex-pressure side leg, which entraps most of the purge air. The increased heat load to the first rotor pushed the designers to exploit this purge flow not only for sealing purposes, but also for cooling ones. Typically, a purge to mainstream mass flow ratio in the range 0.7–1.0% suffices in effectively sealing the disk cavity from hot gas ingestion, but larger mass fractions could be required for cooling. Indeed, rising the coolant-to-mainstream mass flow rate (*MFR*) has a positive effect on platform cooling (see for example Narzary et al. (2012)). To fully capture all flow and heat transfer phenomena related to purge to main flow interaction across the rotor, investigations on rotating rigs (Schuepbach et al. (2008) among others) and stationary blade

cascades (e.g. Popovic et al. (2013)) have been performed over the years. Only few researches investigated the impact of variable rotational speed (Suryanarayanan et al. (2010)), and of slot dimension and shape variation (e.g. Lynch et al. (2017) and Barigozzi et al. (2013)). At the author's best knowledge, the impact of mainstream incidence variation has never been investigated before.

Turbine operating conditions can change due to a different load requirement, but also due to different ambient conditions. Whatever the motivation, a reduced mass flow, at fixed rotational speed, translates into a negative incidence to the first rotor blade cascade for a subsonic flow condition, resulting in a reduction of secondary flows and related losses (Perdichizzi (1989)). But incidence along the blade span can significantly vary, due to the complex flow coming from the stator, resulting from the interaction between swirling combustion gases, coolant flow emerging from the combustor to stator interface gap and stator secondary flows (Abdeh et al. (2019), Chen et al. (2017) and Schreiner et al. (2020)). All these make the flow pattern interacting with the sealing flow emerging from the stator to rotor interface gap highly complicated, impacting its sealing and cooling capabilities. Last but not least, reducing the operability of the turbine to the minimum load, could result into a mismatch between what the compressor can deliver to the SAS and what the turbine requires for sealing, potentially compromising the safe operation of the whole engine.

This study experimentally investigates the aerodynamic behavior of a rotor blade cascade with platform cooling through an upstream slot under different incidence angles from nominal to -20°, representing possible off-design flow conditions down to the minimum load. For discrete values of this parameter, the coolant to mainstream mass flow rate *MFR* was varied at fixed $DR = 1.0$, $Tu_1 = 7.5\%$ and $Ma_{2is} = 0.55$. The decision to keep the main flow rate at a fixed level was motivated by the desire to isolate the effect of incidence. Indeed, varying the main flow rate would have resulted in a combined change in Reynolds number and Mach number, making it difficult to identify the different contributions. On the other hand, the presented results constitute a starting point of a wider investigation whose aim is to assess the impact of off-design conditions on both aerodynamic and heat transfer behavior of a rotor blade cascade, also considering gap geometrical modifications.

EXPERIMENTAL SETUP

The experimental campaign was carried out at the continuous running, suction type wind tunnel for rotor blade cascades shown in Fig. 1. This facility and the cascade model (Fig. 2) have been deeply described in Barigozzi et al. (2019), even if some upgrades have been implemented, mostly on the fan section, allowing to reach a much higher exit Mach number. The wind tunnel test section hosts a 7-blade cascade typical of first high-pressure turbines: the cascade is characterized by a pitch-to-chord ratio of 0.637 and an aspect ratio of 1.24 (Table 1). The profile of the cylindrical airfoil (Fig. 2) replicates the hub section of an industrial first rotor airfoil. Similarly, the blade to hub junction is made through a 3D fillet, replicating the real engine design.

Tests were carried out at a fixed inlet Mach number $Ma_1 = 0.24$, roughly corresponding to a downstream isentropic Mach number $Ma_{2is} = 0.55$, varying the inlet flow angle from 0° incidence down to -20° incidence, with a regular step of 10°. To obtain these discrete incidence variations (-20°, -10°, 0°), the wind tunnel inlet section was re-designed. Figure 3 shows the picture of the lowest tested incidence setup ($i = -20°$).

The wind tunnel was run in steady state conditions at high inlet turbulence intensity ($Tu_1 = 7.5\%$). A grid formed by cylindrical rods was used to increase the inlet turbulence intensity. Turbulence decay was found to be consistent with that shown in Barigozzi et al. (2019), providing a 7.5% Tu_1 level at the leading edge plane, as verified by a 2D LDV probe.

Inlet flow condition was monitored 1.0 C_{ax} upstream of the leading edge plane using a 3-hole aerodynamic probe, while exit conditions were monitored by a set of 31 pressure taps distributed over four passages in the tangential direction at a distance of $0.5C_{ax}$ from the trailing edge plane. The inlet flow was also characterized in terms of velocity profile and turbulence content. Figure 4 shows the inlet boundary layer profile measured by means of a flattened pitot probe ($\delta Ma = \pm 0.01$); integral parameters, turbulence intensity and integral length scale Λ_x, acquired by a single wire hot

wire probe, are also reported. The integral length scale was computed numerically integrating the autocorrelation function of the acquired hot wire signal.

Rotor platform cooling is accomplished by a slot simulating the stator to rotor interface gap (Fig. 5). Slot width is $0.042C$ and it is located $0.158C_{ax}$ upstream of the leading edge plane, covering three and a half blade passages (see Fig. 2). To give the purge flow the proper injection angle, 8 fins were installed inside the slot. The same cooling scheme has been previously tested by the authors in a different rotor blade cascade at a lower Ma_{2is} of 0.3 and Tu_1 of 0.6% (Barigozzi et al. (2014)). The fins inclination angle has to be selected to simulate as close as possible the combined influence of rotation and injection condition. As a general rule, keeping a fixed rotational speed, doubling the *MFR* would roughly result in also doubling the tangential injection angle. The nominal value of -10° here considered (see Fig. 5 - right) was originally selected to be representative of the engine operating conditions with a 1.0% *MFR*.

Testing conditions included variations of *MFR* up to 2.0%, injecting air at room temperature as coolant. The investigated *MFR* range is large enough to cover any possible engine operating condition. Coolant mass flow (orifice device - δm_c<±2.1%), total pressure (δp_c=±10Pa) and temperature (δT_c=±0.5°C) inside the plenum were monitored to control the injection conditions. A confidence interval of 95% was always considered for all uncertainty evaluations.

Fig.1. Wind tunnel.

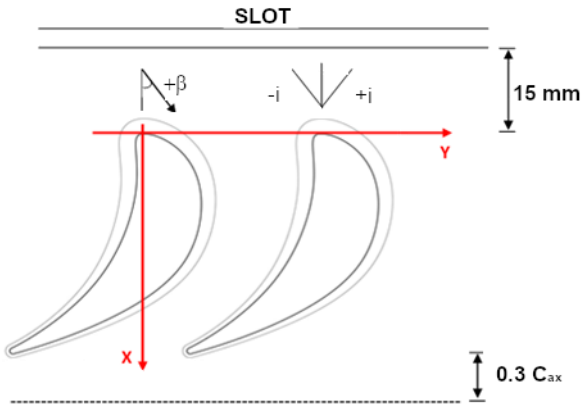

Fig.2. Rotor blade cascade.

Table 1. Cascade geometry and nominal operating conditions

s/C =0.637	Ma_{2is} = 0.55
H/C = 1.24	Tu_1 = 7.5%
β_1 = -30.87°	Re_{2is} = 1.51x10^6

Fig. 3. Setup for *i* = -20°.

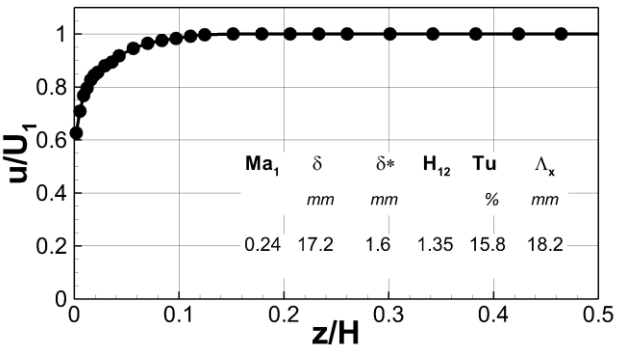

Fig. 4. Inlet boundary layer (X/C_{ax} = -1).

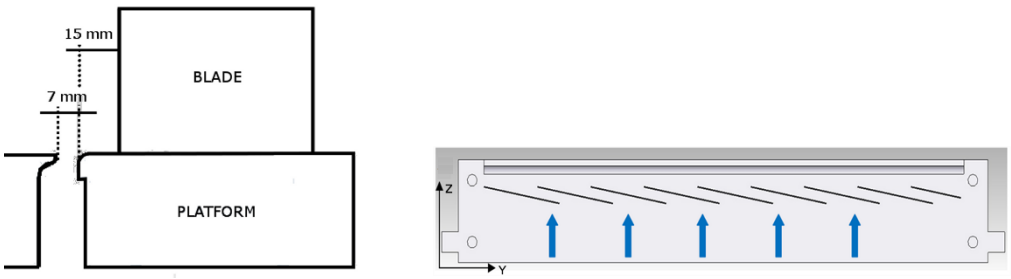

Fig. 5. Platform cooling schemes.

MEASUREMENT TECHNIQUES

Each wind tunnel setup was first tested to assess the actual inlet flow angle and, thus, the incidence to the cascade. Moreover, the purge flow emerging from the slot was also characterized in design cascade condition when MFR = 1%. This to verify its injection angle and even distribution between adjacent passages. The blade to blade mid span flow in the cascade entrance region and the slot mid-height section were characterized by a 2D LDV system. The light source was a 300 mW Ar+ laser. All measurements were carried out acquiring 20,000 burst signals at each location. Sawdust smoke was used to seed the flow. The high number of acquired signals assured statistically accurate averages: based on a 95% confidence level, uncertainties of ±0.14% and ±1.0% for mean and RMS values, respectively, have been obtained for a turbulence intensity level of 10%.

The combined impact of mainstream incidence and platform cooling on the aerodynamics of the cascade flow was assessed by traversing a miniaturized 5-hole aerodynamic pressure probe (2mm head diameter, advanced 50 mm from the stem) at 30% of the axial chord downstream of the trailing edge plane. The probe was in-house calibrated over a wide range of Mach numbers (0.05-0.7) as well as yaw and pitch angles (±25°). Traverses extend over two pitches, covering half of the blade span. Distributions of kinetic energy loss coefficient ($\delta\zeta$ = ±0.3%), deviation angle $\Delta\beta$ ($\delta\beta$ = ±1°) and streamwise vorticity Ω_s were derived from local data. The latter was normalized using the inlet flow velocity and the true chord.

RESULTS

The experimental results provided information regarding the aerodynamic behavior of the considered rotor platform cooling scheme at variable MFR, in the range between 0.5% and 2.0%, and variable inlet flow incidence from nominal down to -20°. To follow, the inlet flow and slot exit flow characterization are first described, to estimate the actual incidence to the cascade, then the influence of incidence on secondary flows losses are discussed, taking the uncooled case as a reference.

Cascade inlet flow characterization

Figure 6 shows the pitch wise profiles of Mach number and flow angle measured at X/C_{ax} = -0.5 for the three tested incidence values. This upstream location was selected since it is far enough from the blade leading edge to be not influenced by stagnation effect. Inlet flow angle β is defined with respect to the axial direction: according to Craig and Cox (1971) incidence definition, a negative incidence corresponds to an inlet flow angle larger, or less negative, than in the design case. The pitch wise flow distributions show a good stability in the cascade entrance region and a good consistency between the different incidence cases in terms of inlet Mach number, being the averaged inlet Mach number Ma_1 always about 0.24, with a maximum variation of the order of ±1.5% over two pitches. Table 2 reports the actual incidence angles obtained averaging the inlet flow angle values over the two pitches and taking the one measured at the theoretical 0° incidence case as a reference. The turbulence generator induces a flow deviation upstream of the cascade providing a slightly negative incidence at the theoretical 0° incidence, similarly to Chavez et al. (2016) and Abdeh et al. (2019).

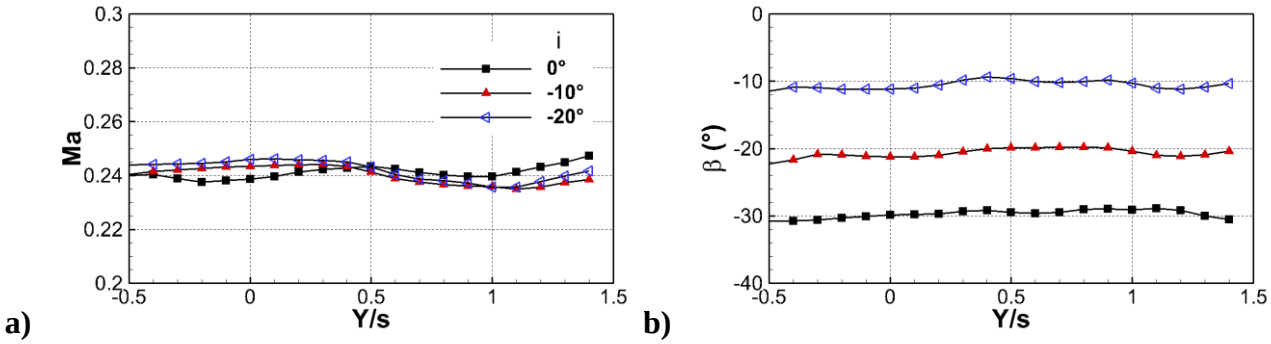

Fig. 6. Approaching flow characterization (X/C_{ax} = - 0.5): a) Ma_1 and b) β.

Table 2. Inlet incidence angle for variable testing conditions

***i* theoretical** (°)	β (°)	***i* actual** (°)
0	-29.8	-1.1
-10	-20.8	-10.1
-20	-10.6	-20.3

Purge flow characterization

To check the quality of purge flow ejection from the slot, coolant flow velocity was measured by the LDV system at slot exit mid section. Tests were carried out for a coolant to mainstream mass flow rate ratio *MFR* = 1.0 % at design incidence. Figure 7 shows that purge flow discharged by the slot is sufficiently periodic in pitch wise direction. Pitch to pitch variation in the three velocity components were always below ±5.5%. The stagnation effect in front of the blades is evident at Y/s = 0 and 1. The average purge flow angle in the (Y,Z) plane was about 12°.

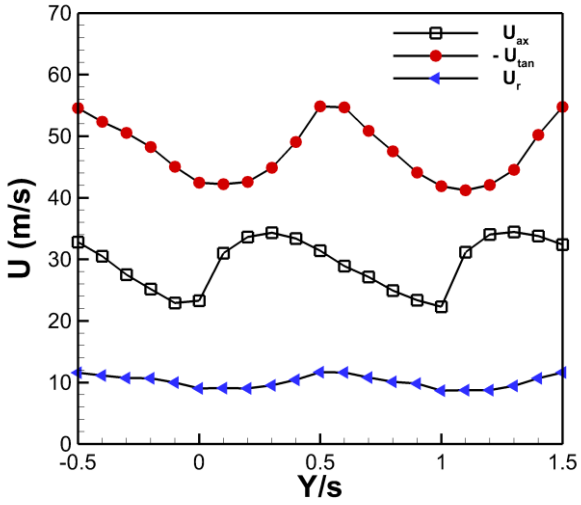

Fig. 7. Purge flow characterization at slot exit (i = 0°).

Local flow behavior – uncooled cascade

Figures 8 and 9 show the kinetic energy loss coefficient (ζ) distributions and the normalized vorticity (Ω) with superimposed the secondary velocity vectors measured downstream of the trailing edge plane for the design (i = 0°) and the minimum tested incidence angle of -20° with a continuous platform (i.e. without slot). The -10° incidence case is not reported since it is close to the design case. These data will be considered as a reference for the following cooled platform investigation.

Two passages are reported to appreciate the flow periodicity at both incidence values tested. Maximum pitch to pitch variation of the order of $\Delta\zeta/\zeta = \pm 4\%$ do exist. At design incidence the flow downstream of the cascade is characterized by a well-defined passage vortex structure that can be easily identified both from the loss concentration on the suction side of the wakes between Z = 0.1 and 0.2 *H* (Fig. 8a) and the negative vorticity region in Fig. 9a. The counter-clockwise rotating vortical structure with the corresponding positive vorticity related to the trailing shed vortex can be also identified in Fig. 8a and 9a. An indication of the presence of corner vortex can be also seen, corresponding to a second region of high loss close to the wall. A significant passage vortex related cross flow can be also identified at the wall proximity.

As expected, according with the literature (see for example Perdichizzi (1989)), an incidence decrease to negative values gives rise to a reduction of secondary flows. The passage vortex related loss peaks keep the same intensity, but move towards the wall, while the corner vortex intensity reduces (Fig. 8b). Vorticity also attenuates together with the endwall cross flow (Fig. 9b).

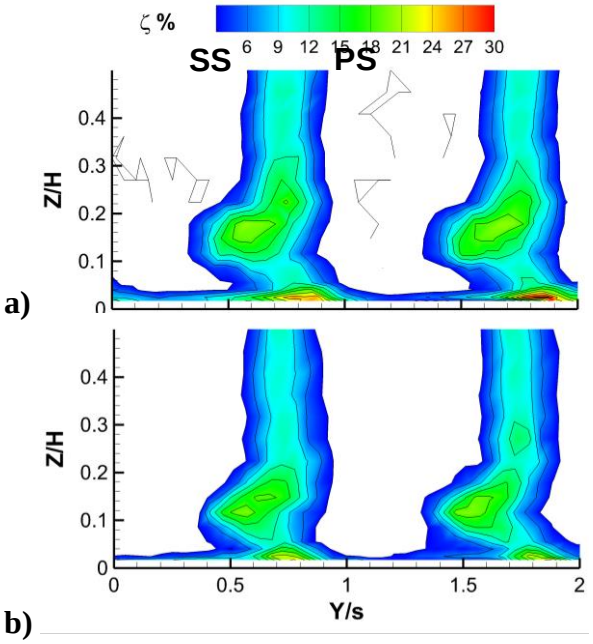

Fig. 8. kinetic energy loss coefficient distributions: a) 0° and b) -20° incidence.

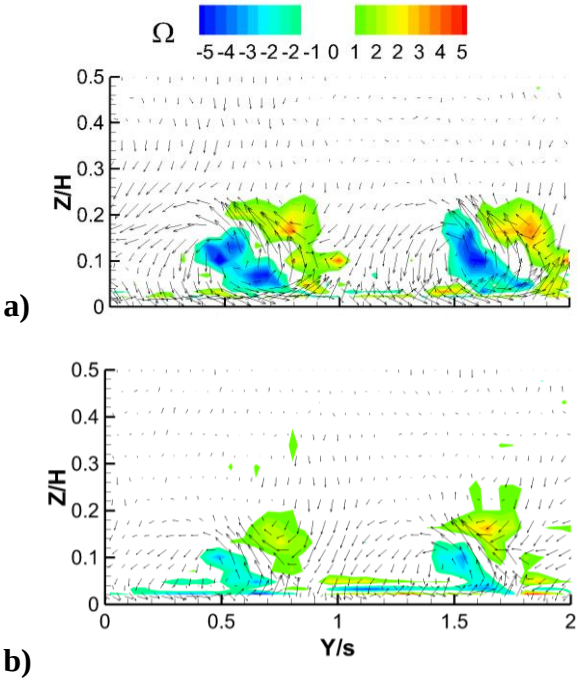

Fig. 9. Vorticity and secondary velocity vectors: a) 0° and b) -20° incidence.

Local flow behavior – cooled cascade

Figure 10 shows the impact of incidence variation (from 0° down to -20°) at fixed cascade operating condition (Ma_1 = 0.24 and Tu_1 = 7.5%) for the tested coolant to mainstream mass flow ratio *MFR* values (from 0.5% to 2.0%). Only one pitch is shown, thanks to the good flow periodicity. Figure 11 reports the corresponding vorticity distributions with superimposed the secondary velocity vectors. For safe of space, only vorticity data belonging to the design (0°) and -20° incidence are reported, as they allow to discuss the general trend even for the -10° case.

As expected, at design incidence (Fig. 10a) coolant injection always increases the kinetic energy losses, the greater the injected mass flow, the more so. Coolant injection with a negative tangential velocity component (i.e. in the same direction of the passage vortex related endwall cross flow) enforces the passage vortex that lifts from the wall, resulting in a highly three-dimensional flow structure leaving the cascade. This behavior is consistent with the vorticity distributions shown in Fig. 11a for the same testing conditions. The measurement plane is dominated by the passage vortex motion providing the subsequent stator a highly skewed approaching flow. The negative vorticity core corresponding to the trailing shed vortex slightly widen, increasing injection, and moves towards midspan, following the passage vortex displacement.

Reducing the incidence angle to -10° and -20° results in a similar behavior when injecting the purge flow at rising *MFR* (Fig. 10b,c and 11b). But even if the trend is similar for the two tested negative incidence values, the impact on the loss behavior is different. Thanks to the beneficial effect of negative incidence, the passage vortex related loss core moves back to the wall and reduces in intensity and size reducing *i*, as also shown by the vorticity contour maps of Fig. 11b. For example, at an *MFR* of 2.0% the loss peak decreases from about 25% at 0° to 23% at -10° down to about 15% at -20°. Moreover, at the same *MFR* of 2% and *i* of -20° a 2D wake is established at mid span section, even if with a limited radial extension. Moreover, the corner vortex trace moves tangentially when incidence reduces from 0° to -10°, as a consequence of the reduced end wall crossflow. A further incidence reduction seems to have a marginal impact on the corner vortex.

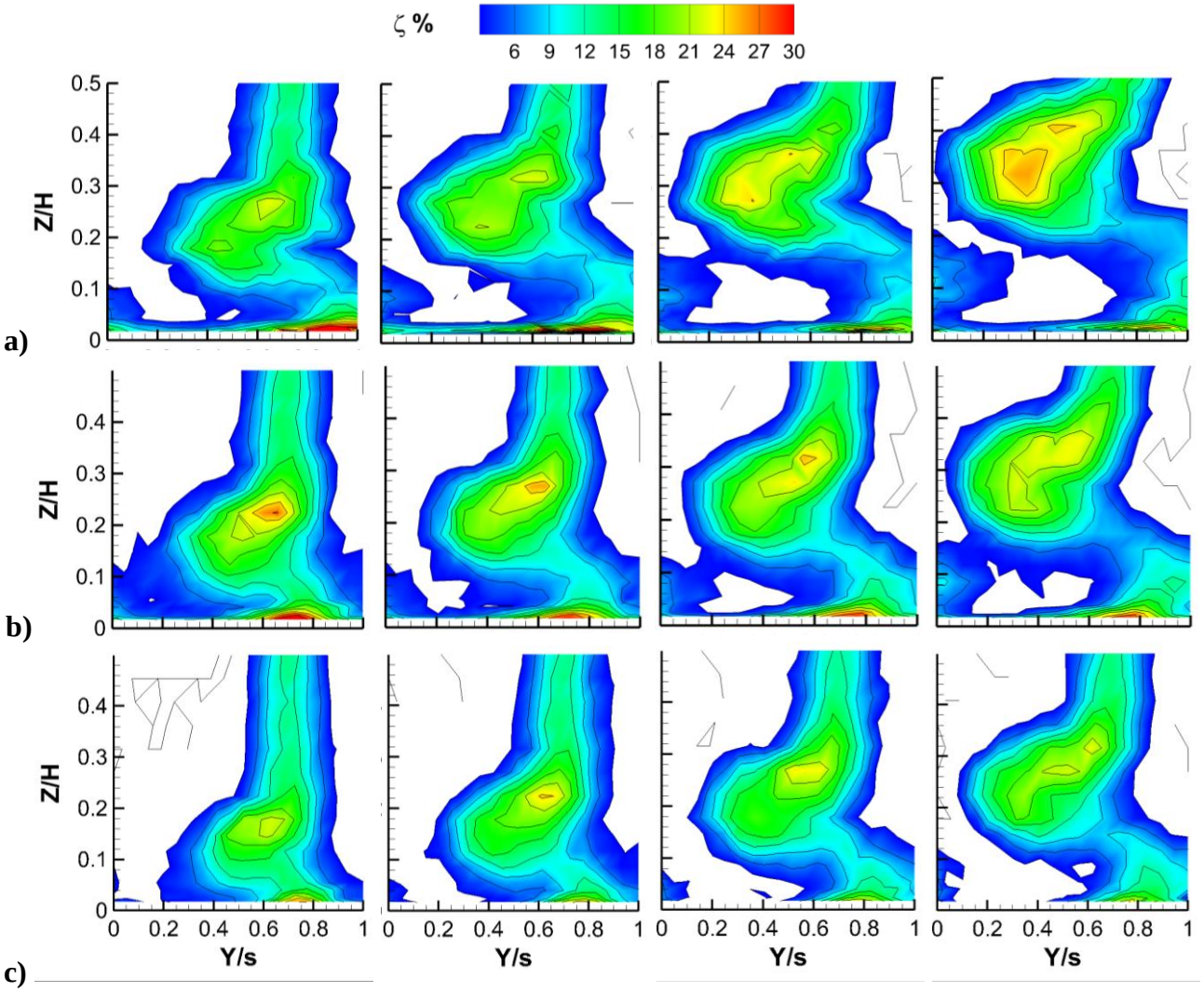

Fig. 10. Kinetic energy loss coefficient distributions for variable *MFR*: a) 0°, b) -10° and c) -20° incidence.

Span-averaged loss and deviation angle

To calculate the span averaged distributions of kinetic energy loss coefficient and deviation angle, local data coming from Fig. 10 and 11 (Fig. 8 and 9 for the solid case) were mass averaged over the pitch. The results are shown in Fig. 12 and 13. Reference data related to the uncooled case (no gap - solid end wall) are also reported (dashed lines). At 0° incidence, a rise in the *MFR* resulted in the increase of the passage vortex loss peak from 6% at *MFR*=0.5% to 8.5% at *MFR*=2.0%, and in the migration of the same towards mid span. Both underturning and overturning values increase

up to -/+ 6°, with angle variations all over the investigated half span. At -10° incidence, a similar behavior is observed, even if with some differences: at small injection rates, the increase in deviation angle is reduced when compared to the design case. Loss increase is similar to the 0° case, but the passage vortex related loss peak is closer to the wall. At high injection rates a similar overturning and underturning is observed, but its spanwise extension is reduced. Something similar happens also at the -20° incidence case, with a further loss reduction (the loss peak at *MFR*=2.0% is now about 7.5% against 8.5% of the 0° case) and shift towards the end wall, that also characterize overturning and underturning.

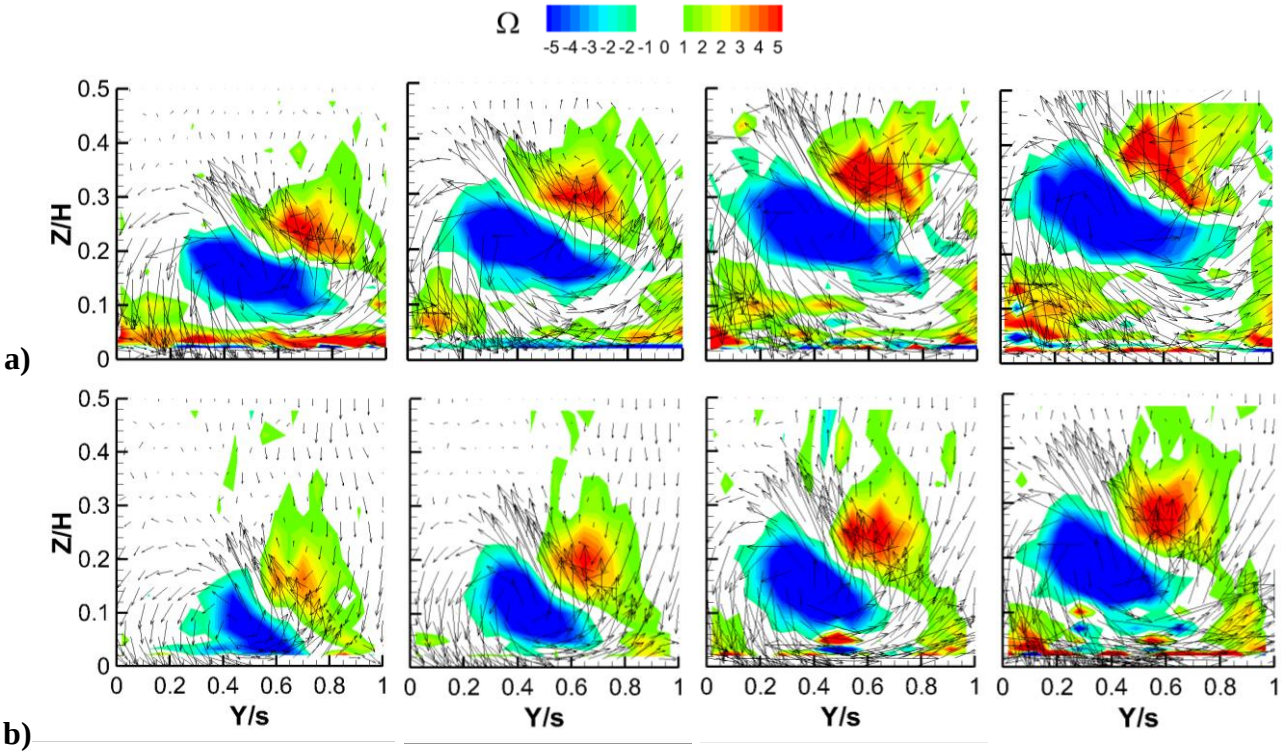

MFR = 0.5% **MFR = 1%** **MFR = 1.5%** **MFR = 2%**

Fig. 11. Ω distributions for variable *MFR*: a) 0° and b) -20° incidence.

Finally, Fig. 12d and 13d compare the pitch averaged deviation angle and loss coefficient variations along the span at a fixed *MFR* = 1% and variable incidence. These pictures clearly show that injecting the purge flow at 0° incidence results in a significant increase in aerodynamic loss and a huge change in the mean flow angle distribution in the spanwise direction at the exit of the cascade, which could be detrimental to the following stator. Reducing the incidence seems to be advantageous as it reduces losses and helps to confine the change in deviation angle to the end wall region.

Overall loss

To allow a more quantitative comparison between the tested operating conditions, overall mass averaged energy loss coefficients were computed from flow field data. The so-called primary loss coefficient has been computed as follows:

$$\bar{\bar{\zeta}} = \frac{\bar{\bar{U}}_{2is}^2 - \bar{\bar{U}}_2^2}{\bar{U}_{2is,ms}^2} \qquad (1)$$

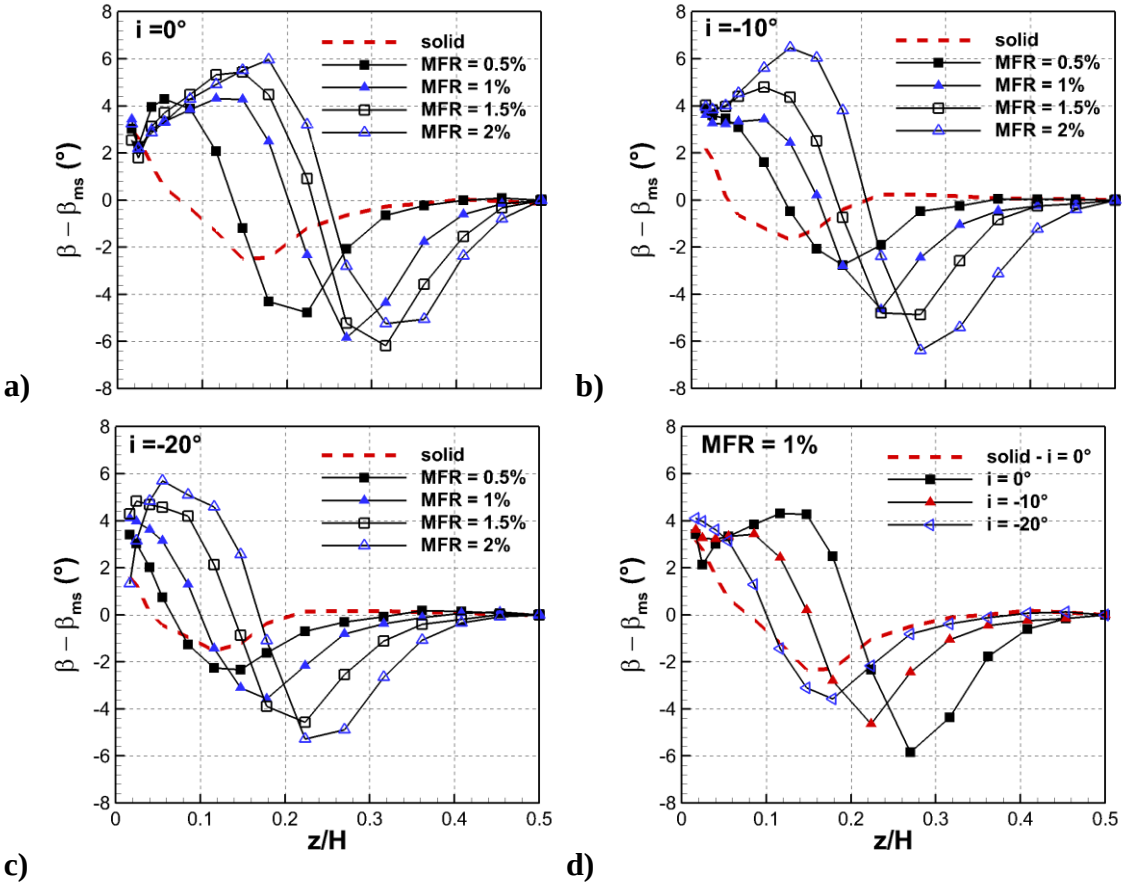

Fig. 12. Δβ for variable *MFR*: a) 0°, b) -10°, c) -20° and d) at fixed *MFR* = 1% and variable *i*.

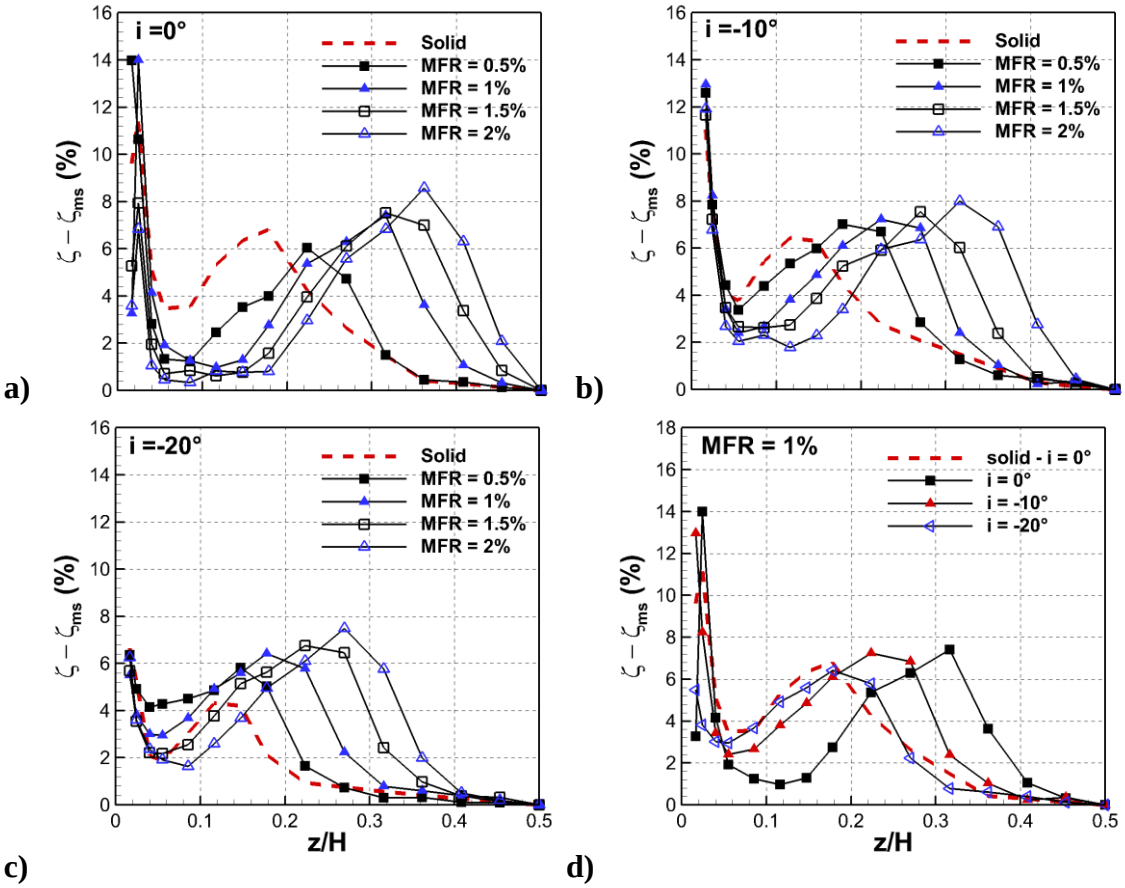

Fig. 13. ζ for variable *MFR*: a) 0°, b) -10°, c) -20° and d) at fixed *MFR* = 1% and variable *i*.

This definition was adopted because the calculated values almost coincide with the thermodynamic loss formulation, which also includes coolant internal losses. A maximum difference of 0.44% was observed at *MFR*=2.0%. Figure 14 shows the overall mass averaged kinetic energy loss coefficient for variable *MFR* at constant incidence. As expected, the overall loss coefficient continuously increases rising the *MFR*, whatever the incidence. Changing the incidence towards negative values does not modify this general behavior, but lowers the loss level, especially at -20°. The impact of a -10° incidence is limited, reducing the overall loss coefficient of about -0.5% whatever the *MFR*. The loss reduction at -20° is much higher, and not constant, reaching -1.6% at *MFR* = 2%.

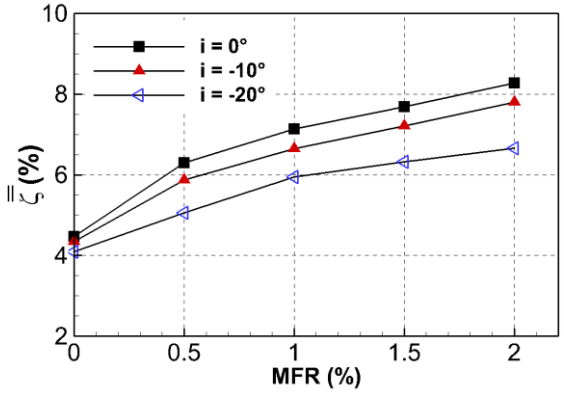

Fig. 14. Overall ζ for variable *MFR* and *i*.

CONCLUSIONS

Aerodynamic measurements were carried out in a rotor cascade under realistic engine conditions (Tu_1 = 7.5%, Ma_{2is} = 0.55) to evaluate the performance of a platform cooling scheme simulating the stator to rotor interface gap at various *MFR* values between 0.5% and 2% with main flow incidence angles of 0°, -10° and -20°. The objective was to evaluate the aerodynamic performance of this cooled blade cascade, by simulating some effects of low load operating conditions. The key highlights of the present study are the following:

- as expected, negative incidence reduces secondary flows generation and development across the cascade, reduces the endwall cross flow and overall losses;
- in the investigated *MFR* range, increasing the coolant flow rate is detrimental to the cascade performance, the larger the loss the higher the injected mass flow. This whatever the incidence to the cascade. In the worst case, i.e. at design incidence, doubling the *MFR* from 1% to 2% resulted in a loss increase of $\Delta\zeta$ = +1.1%.
- the combination of negative incidence and coolant injection only marginally reduces loss production at a moderate incidence of -10° ($\Delta\zeta$ = -0.5% as an average);
- a stronger reduction in *i* down to -20° results in a significant reduction of overall losses, particularly significant at high *MFR*. When *MFR* = 2%, the loss reduction becomes $\Delta\zeta$ = -1.6%;
- in presence of a moderate negative incidence, high *MFR* values could not only be responsible for a huge loss generation, but also for a deterioration of flow quality approaching the following stator, due to huge variations in the spanwise distribution of $\Delta\beta$.

REFERENCES

Abdeh, H., Barigozzi, G., Perdichizzi, A., Henze, M., Krueckels, J., (2019). *Incidence Effect on the Aero-Thermal Performance of a Film Cooled Nozzle Vane Cascade*. J. Turbomach. 141.

Barigozzi, G., Franchini, G., Perdichizzi, A., Maritano, M., Abram, R., (2013). *Purge flow and interface gap geometry influence on the aero-thermal performance of a rotor blade cascade*. Int. J. of Heat and Fluid Flow 44.

Barigozzi, G., Franchini, G., Perdichizzi, A., Maritano, M., Abram, R., (2014). *Influence of purge flow injection angle on the aerothermal performance of a rotor blade cascade*. J. Turbomach. 136.

Barigozzi, G., Perdichizzi, A., Pestelli, L., Abram, R., (2019). *Combined Experimental and Numerical Investigation of the Aero-Thermal Performance of a Rotor Blade Cascade with Platform Cooling*. Proceedings of the ASME Turbo Expo 2019: Turbomachinery Technical Conference and Exposition, Phoenix, Arizona, USA.

Barigozzi, G., Abdeh, H., Rouina, S. Franchina, N., (2022), *The Aero-Thermal Performance of Purge Flow and Discrete Holes Film Cooling of Rotor Blade Platform in Modern High Pressure Gas Turbines: A Review*. Int. J. Turbomach. Propuls. Power, 7(3), 22.

Bozzi, L., D'Angelo, E., Facchini, B., Micio, M., Da Soghe, R., (2011). *Experimental Investigation on Leakage Losses and Heat Transfer in a Non- Conventional Labyrinth Seal*. ASME Paper GT2011-46362.

BP Statistical Review of World Energy 2022, 71st edition

Chavez, K.F., Packard, G.R., Slavens, T.N., Bogard, D.G., (2016). *Experimentally Determined External Heat Transfer Coefficient of a New Turbine Airfoil Design at Varying Incidence Angles*. Proceedings of ISROMAC 2016.

Chen, A. F., Shiau, C. C., Han, J. C., (2017). *Turbine blade platform film cooling with simulated swirl purge flow and slashface leakage conditions*. J. Turbomach. 139.

Craig, H.R.M. and Cox, H.J.A., (1971). *Performance Estimation of Axial Flow Turbines.* Proc Instn Mech Engrs, 187, pp.32-71.

Fraczek, D., Bochon, K., Wroblewski, W., (2016). *Influence of Honeycomb Land Geometry on Seal Performance*. ASME Paper GT2016-57569.

Lynch, S. P. and Thole, K. A., (2017). *Heat Transfer and film cooling on a contoured blade endwall with platform gap leakage*, J. Turbomach. 139.

Narzary, D. P., Liu, K. C., Rallabandi, A. P., Han, J. C., (2012). *Influence of coolant density on turbine blade film-cooling using pressure sensitive paint technique*. J. Turbomach. 134.

Nayak, K.C., (2020). *Effect of Rotation on Leakage and Windage Heating in Labyrinth Seals with Honeycomb Lands*. J. Eng. Gas Turbines & Power 142.

Perdichizzi, A., (1989). *Mach Number Effects on Secondary Flow Development Downstream of a Turbine Cascade*. Proceedings of the ASME 1989 International Gas Turbine and Aeroengine Congress and Exposition, Toronto, Ontario, Canada.

Popovíc, I., Hodson, H. P., Janke, E., Wolf, T., (2013). *Aerothermal impact of the interaction between hub leakage and mainstream flows in highly-loaded high pressure turbine blades*. J. Turbomach. 135.

Ray A, De S. *Renewable Electricity Generation – Effect on GHG Emission. Encyclopedia of Renewable and Sustainable Materials*, Elsevier; 2020, p. 728–35.

Regina K. and Kalfas, A. I., (2015). *Experimental investigation of purge flow effects on a high pressure turbine stage*. J. Turbomach. 135.

Schreiner, B. D., Wilson, M., Li, Y. S., Sangan, C. M., (2020). *Effect of Purge on the Secondary Flow-Field of a Gas Turbine Blade-Row*. J. Turbomach. 142.

Schuepbach, R. S., Abhari, M. G., Rose, T., Germain, I., Raab, J. G., (2008). *Effects of Suction and Injection Purge-Flow on the Secondary Flow Structures of a High-Work Turbine*. ASME Paper GT2008-50471.

Suryanarayanan, A., Mhetras, S. P., Schobeiri, M. T., Han, J. C., (2010). *Film-Cooling Effectiveness on a Rotating Turbine Platform using Pressure Sensitive Paint Technique*. J. Turbomach. 132.

Szyma´nski, A., Wroblewski, W., Bochon, K., Majkut, M., Strozik, M., Marugi, K., (2020). *Experimental validation of optimised straight-through labyrinth seals with various land structures*. Int. J. Heat & Mass Transfer 158.